Proceedings of the Sixteenth International Conference on
Computational Structures Technology
Edited by: P. Iványi, J. Kruis and B.H.V. Topping
Civil-Comp Conferences, Volume 14, Paper 14.2
Civil-Comp Press, Edinburgh, United Kingdom, 2026
ISSN: 2753-3239, doi: 10.4203/ccc.14.14.2

Reduced Mesoscale Modelling for Masonry Arch Bridges

M. S. El Ashri[1,2], S. Grosman[1,2], L. Macorini[1] and B. A. Izzuddin[1]

[1]Department of Civil and Environmental Engineering, Imperial College London, United Kingdom
[2]School of Engineering and Design, London South Bank University, United Kingdom

Abstract

This paper introduces a reduced mesoscale modelling approach for the accurate and efficient assessment of old masonry bridges. As these ageing structures remain a vital part of Europe's infrastructure, they must be assessed under current traffic loads using models that accurately capture the characteristic 3D response and the anisotropic behaviour arising from the actual masonry bond of the key bridge components. This can be achieved through detailed, high-fidelity 3D masonry models, though these can pose excessive computational demands, thereby constraining their practical application. Typically, more simplified models are used, either employing 3D macroscale isotropic approaches or 2D models that omit 3D effects, potentially leading to inaccurate response predictions. To improve this, the paper utilises mesoscale masonry models with relaxed bond patterns. Numerical results show that bridge models with a calibrated, reduced mesoscale mesh for the masonry parts of the bridge achieve performance comparable to full mesoscale models, capturing essential features of the response to vertical loading while significantly reducing the computational demand.

Keywords: masonry arch bridges, structural assessment, computational efficiency, reduced mesoscale models, material properties calibration, ageing infrastructure.

1 Introduction

Masonry arch bridges make up a significant portion of the bridge stock for Europe's transport network. These bridges were designed using empirical rules and were not intended to withstand continuously increasing traffic loads. Moreover, their prolonged exposure to harsh environmental conditions has further contributed to their deterioration. As a result, there is an urgent need for reliable assessment tools that can accurately evaluate the performance of these bridges. Such tools can help implement effective strengthening/repair measures to improve the performance of substandard bridges or restrict current traffic loads to safe levels.

Masonry bridges are heterogeneous structures comprising various components, leading to complex interactions between structural and non-structural parts, as observed in previous experimental investigations [1-6]. To capture the actual 3D response, detailed high-fidelity 3D modelling approaches based on the finite element method (FE) [7-10] or discrete element method (DEM) [11-15] can be adopted. However, these methods involve high computational costs, limiting their practical applicability. This creates a need for computationally efficient models.

Previous investigations on simplified assessment methods for masonry bridges vary in several aspects, such as dimensionality (2D or 3D), masonry modelling strategy (continuum or discrete), and analysis type (rigid-plastic or incremental elasto-plastic). For instance, limit analysis was considered in previous studies using either 2D [16, 17] or 3D models [18, 19] to determine the bridge load-carrying capacity and failure mode. However, limit analysis cannot capture the actual response at service-load levels, and it does not provide insights into the sequence of crack formation or displacements that occur at collapse. These shortcomings were partially addressed in [20] by adopting a combined approach that integrates adaptive limit analysis with a discrete FE method. This enables determination of the load-displacement curve through non-linear static analysis, which is performed after the failure mode is identified using limit analysis.

For incremental methods, previous studies have considered using 3D continuum macroscale models [21-23] to investigate the behaviour of masonry arch bridges. In addition, a 3D macroscale homogenised FE modelling strategy was developed in [24] and adopted to study the behaviour of actual bridges under train loading [25]. Finally, Zizi et al. [26] employed 3D macroscale models for multi-span masonry bridges to study the influence of variations in macroscale material parameters and the effects of initial damage on the load capacity of bridges [27].

One limitation of macroscale modelling is its homogenised representation of masonry units and mortar joints. Thus, the constitutive model cannot be calibrated solely by conducting material tests on the individual masonry constituents. Instead, tests should be performed on substantial masonry components to determine the material characteristics of masonry as a uniform composite material, which makes the calibration process more complex. In [28, 29], nonlinear simulations of 2D masonry arch bridges were performed to assess the accuracy of macroscale models relative to detailed mesoscale models, considering both simple and advanced calibration procedures. However, it did not provide consistent results when ring separation failures take place. To enable ring separation, a hybrid macroscale modelling strategy was investigated, accounting for circumferential joints between macroscale masonry rings. This strategy showed very promising results but was tested only on 2D models. This indicates that continuum models are limited in their representation of damage and cracking, which is smeared, making it difficult to identify the exact locations and widths of cracks. This affects their accuracy, especially when failure modes such as ring separation occur.

To overcome this drawback, several attempts have examined the effects of cracking using a qualitative approach to improve computational efficiency compared with detailed models. For example, a macroscale approach with embedded discontinuities was adopted in [30]. Moreover, a 3D discrete macro-element modelling approach (DMEM) for masonry bridges was introduced in [31-34]. This DMEM allows for in-plane shear deformations and interacts with adjacent macro-elements by nonlinear interfaces.

Recent advancements in 3D modelling for masonry arch bridges have yet to fully capture their complete 3D response under varying load levels. Achieving this requires realistic modelling of the masonry bond across all bridge components, as well as accurate simulation of interactions among the different parts of the bridge. The methodology proposed in this paper effectively addresses these critical requirements by using relaxed mesoscale models as a reliable and efficient assessment tool. The relaxed mesh still allows for the actual bond, using fewer solid and nonlinear interface elements than detailed (full) mesoscale models. Furthermore, it implements a straightforward material calibration procedure that links the relaxed mesoscale model material parameters to those of the associated full mesoscale model, which can be derived from simple material tests on masonry constituents.

2 Methods

This paper adopts a relaxed mesoscale modelling strategy for the masonry parts of arch bridges, utilising the discrete 3D mesoscale approach introduced in [35]. This allows for a relaxed mesh representation of the actual masonry bond, while maintaining the main features of the bond pattern. The developed relaxed mesoscale models follow the same approach as the full mesoscale models, utilising elastic solid elements and nonlinear interface elements to represent brick/block masonry. However, in this case, an individual elastic solid element encompasses more than one masonry unit, necessitating calibration of the model material parameters to ensure equivalence with the full mesoscale model. Figure 1 shows different levels of relaxation for the mesoscale mesh of a stretcher (running) bond masonry component. This equivalence concept between full and relaxed mesoscale models is not limited to the stretcher bond but can be applied to any masonry bond pattern. Unlike masonry, a continuous modelling approach is adopted for the backfill, in which 3D elasto-plastic solid elements represent the backfill domain, as outlined in [7]. To account for interactions among the different bridge structural and non-structural components, nonlinear interface elements simulate the physical interfaces connecting the parts, and a mesh-tying approach is adopted to accommodate non-conforming meshes [36]. This modelling strategy [9, 38] is implemented in the nonlinear finite element program ADAPTIC [37].

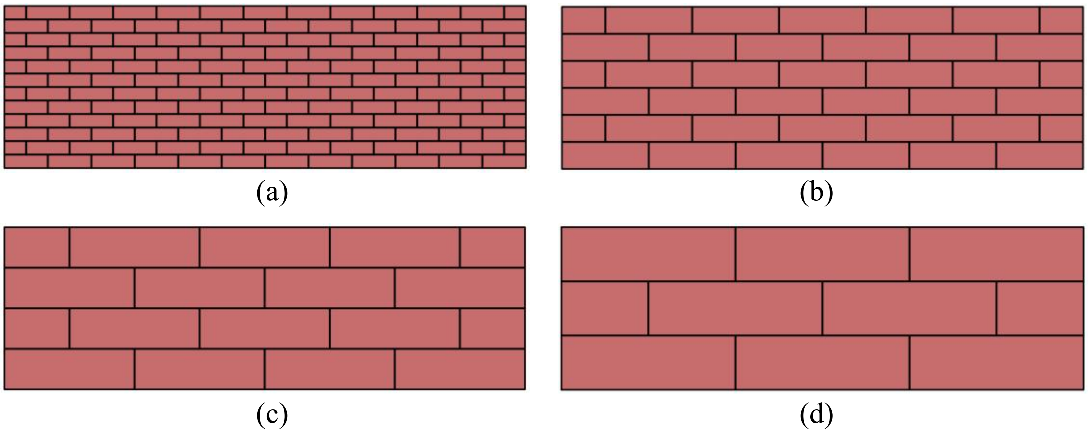

(a) (b) (c) (d)

Figure 1: Different levels of relaxation for stretcher (running) bond masonry; (a) full mesoscale; (b) 2X relaxed; (c) 3X relaxed; (d) 4X relaxed.

In this study, full mesoscale models are used as a baseline to assess the accuracy of simplified relaxed mesoscale models. The full mesoscale models have been validated in [39] using results from physical tests on full-scale single-span masonry bridges with various characteristics and defects conducted at Bolton Institute [2]. In the experimental programme, material tests were also conducted on masonry, mortar, brick, and backfill specimens. The material test results have been used to determine the model material parameters for validating the bridge full mesoscale models. The material parameters are outlined in Table 1, where a detailed description of the calibration procedure is provided in [39].

According to the proposed approach, stiffness equivalence is achieved by varying the stiffness characteristics of the interface elements in the relaxed mesoscale model, depending on the degree of relaxation of the relaxed mesoscale mesh relative to the baseline detailed mesoscale mesh. On the other hand, the same strength material parameters for the interface elements are assumed in the relaxed models, for any level of relaxation. For any brick masonry structure, including masonry arches and walls, the stiffness equivalence needs to be computed individually for each relaxation direction (span, width, and thickness directions, or length, height, and thickness directions for arches and walls, respectively). This is performed assuming the brick units and the mortar joints as linear springs connected in series. Such equivalence for the overall stiffness of both the full and relaxed mesoscale meshes is utilised to derive the unknown stiffness of the interface elements representing the mortar joints in the relaxed mesoscale models along any relaxation direction. Based on this, the normal and shear stiffness values for a reduced mesoscale mesh are given by (1) [39].

Solid Elements						Nonlinear interface elements				
Brickwork			Crushed Limestone					Mortar joints	Brick-to-Brick	Masonry-Backfill
E_b	[N/mm^2]	69000	E_f	[N/mm^2]	200	k_n	[N/mm^3]	295	1E4	40
ν_b	[-]	0.15	c_f	[MPa]	0.001	k_t	[N/mm^3]	118	1E4	20
			φ_f	[Rad]	0.960	f_{ti}	[MPa]	0.21	11.50	0.002
			ψ_f	[Rad]	0.4363	f_{ci}	[MPa]	26.5	115	26.5
						c_i	[MPa]	0.29	16.10	0.003
						G_{ti}	[N/mm]	0.01	0.212	1E5
						G_{si}	[N/mm]	0.029	1.61	1E5
						$\tan(\varphi_i)$	-	0.64	0.00	0.675
						$\tan(\psi_i)$	-	0.00	0.00	0.00

Table 1: Material parameters for solid elements representing the brick units and backfill, and for the nonlinear interface elements for brickwork and the masonry-backfill physical interface adopted in the validated numerical models [39].

where:

E_b & E_f: Young's modulus for bricks and backfill

ψ_f & ψ_i: Dilatancy angle for backfill and interface elements

ν_b: Poisson's ratio for bricks

k_n & k_t: Normal and tangential stiffness for interface elements

c_f & c_i: Cohesion for backfill and interface elements

f_{ti} & f_{ci}: Tensile and compressive strength for interface elements

φ_f & φ_i: Friction angle for backfill and interface elements

G_{ti} & G_{si}: Fracture energy in tension and shear for interface elements

$$K^*_{mj} = \frac{n^*_{mj}}{n_{mj}} \times K_{mj} \tag{1}$$

where:

K_{mj}: Stiffness of mortar joint

n_{mj}: Number of mortar joints

K^*_{mj}: Stiffness of mortar joint (Relaxed)

n^*_{mj}: Number of mortar joints (Relaxed)

3 Numerical results

To investigate the accuracy and computational efficiency that can be achieved by relaxing the mesoscale mesh, an initial study has been conducted using 2D strip models for simulating the response to vertical loading of representative masonry arch bridges. In the investigation, the reduction of the mesoscale masonry mesh is applied along the span direction, the thickness direction, and the span and the thickness directions simultaneously.

The performance of the different relaxed models has been assessed against the full mesoscale models using two sets of material parameters to appreciate the importance of calibrating the stiffness parameters for the interface elements. The first set represents the uncalibrated stiffness parameters (unchanged baseline full mesoscale parameters), while the second set represents the calibrated stiffness parameters, which are calculated as described in the previous section. The motivation for this stems from the fact that most previous studies that adopt discrete modelling strategies for masonry [12-14] to analyse large masonry structures do not consider an exact, detailed representation of masonry bonds. In these models, relaxed meshes with far fewer rigid or deformable blocks than the actual number of masonry units in the analysed structure were employed to improve computational efficiency and facilitate mesh development. Notably, the material parameters were typically calibrated based on the masonry response at the macroscale, without leveraging one of the main benefits of mesoscale masonry modelling, in which the material properties are obtained from simple mechanical tests on the masonry constituents.

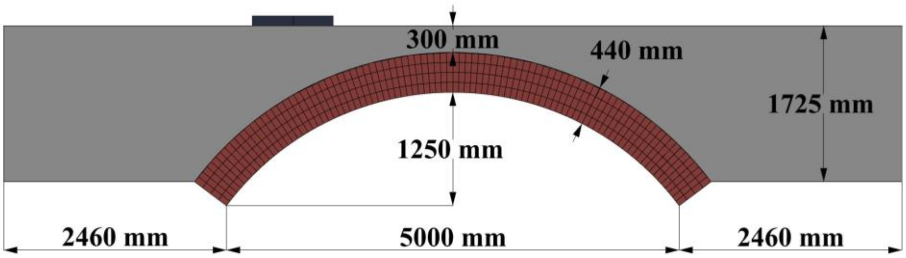

Figure 2: 5 m span 4-ring bridge with stretcher bond.

Model	Span direction		Thickness direction	
	k_n [N/mm^3]	k_t [N/mm^3]	k_n [N/mm^3]	k_t [N/mm^3]
Uncalibrated	295	118	295	118
Calibrated (2 Rings)	141.64	56.69	98.33	39.33
Calibrated (3 Rings)	-	-	196.67	78.67

Table 2: Stiffness parameters for the mortar joints in the uncalibrated and calibrated relaxed models with relaxation along the span and arch thickness directions.

The analysed 2D strip model represents a masonry bridge with a 5 m span and a rise-to-span ratio of 1:4. The arch barrel follows the stretcher bond, with four brick masonry rings totalling 440 mm in thickness, while the depth of backfill above the arch crown is 300 mm, as outlined in Figure 2. The load is evenly distributed over a 900 mm length, centred at the quarter- and mid-span. The analysed bridge has a degree of relaxation of 2, where each solid element comprises two brick units (e.g., Relaxed 2X in Figure 1). Both the uncalibrated and calibrated stiffness parameters in Table 2 have been adopted for the interface elements representing mortar joints in the relaxed models to assess the effects of the model calibration. The results obtained by reducing the mesoscale mesh along the span direction and by reducing the thickness, and by reducing both span and thickness, have been compared against the predictions provided by the full mesoscale model.

The load-displacement curves for the two load positions are shown in Figure 3, where peak load and secant stiffness errors from the full mesoscale predictions are used to assess the accuracy of the relaxed models. The results confirm that the relaxed calibrated models provide a reasonable estimate of the performance under serviceability loading, with a maximum secant stiffness error of 14% when the load is applied at mid-span and for relaxation along both the span (L) and thickness (H) directions. On the other hand, as expected, the uncalibrated models lead to more significant secant stiffness errors for all loading positions and relaxation directions, with a maximum overestimation of 58% for load applied at mid-span with relaxation along the span (L). Regarding the load capacity predictions, the calibration has little impact on the accuracy of the relaxed models. The differences between the uncalibrated and calibrated models are minimal, even though the calibrated models have smaller errors. Importantly, relaxed models provide realistic estimates of the peak load if relaxation is applied only along the span. Once relaxation is introduced along the arch barrel thickness direction, either alone or in conjunction with relaxation along the span, highly overestimated peak load values are obtained for the two load locations, with peak load errors of 24% and 137% when the load is applied at quarter- and mid-span, respectively.

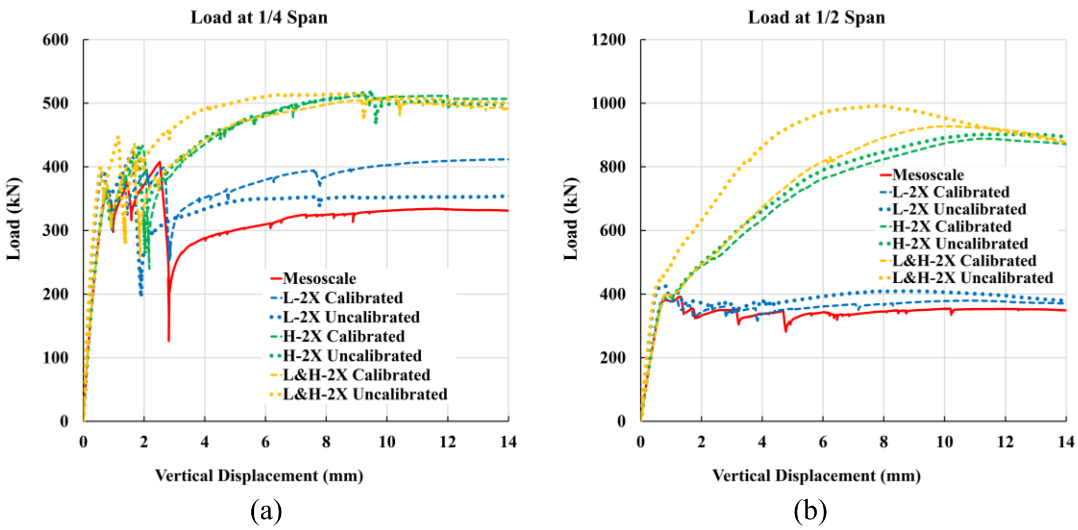

Figure 3: Load-displacement curves for calibrated and uncalibrated 2D relaxed models with 2X relaxation in three alternative directions (L, H, L&H) against full mesoscale models under vertical load applied at (a) quarter; (b) mid-span.

After assessing the influence of calibration on the relaxed models and on the different forms of relaxation on both load capacity and bridge stiffness, the focus now turns to the failure mode. The deformed shapes at failure under the quarter-span load in Figure 4 generally show a good agreement between the different relaxed models and the reference full mesoscale model. The failure mechanism with four hinges and ring separation is captured by all models under the quarter-span load in Figure 4. However, the relaxed model with coarser meshes cannot predict the complex crack orientations along radial and circumferential mortar joints, especially when relaxation is applied in the thickness direction. In this case, the reduced models with only one circumferential mortar joint seem inadequate to fully represent the analysed bridge, which has a 4-ring stretcher-bond arch. This is also reflected in the higher load capacities of the reduced model with relaxation along the arch thickness, as pointed out before, which may indicate that a simple stiffness calibration is not sufficient to represent the full response to collapse.

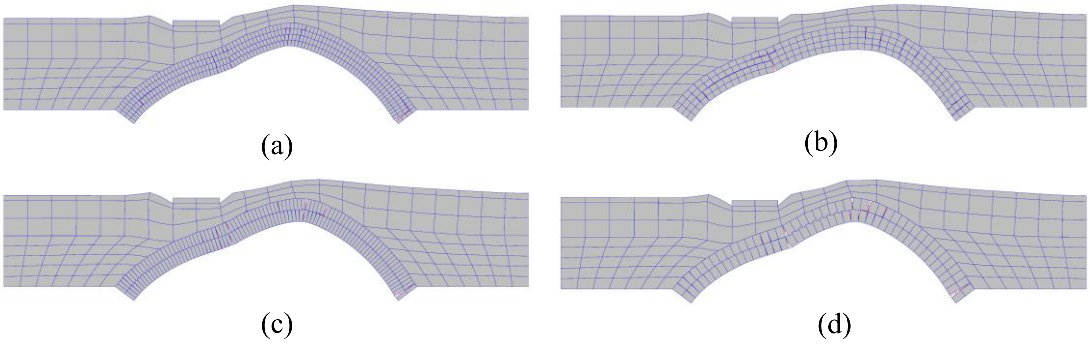

Figure 4: Deformed shapes at failure for 2D strip models under load at quarter span for (a) full mesoscale; and 2X relaxed (b) along span; (c) along thickness; (d) along both span and thickness.

To better understand the issue of relaxation along the arch thickness direction, the influence of the number of rings in the relaxed models is investigated, considering the same two load positions at quarter- and mid-span in subsequent numerical simulations. The reference case in Figure 2 is considered again, while the relaxation in this case is only along the thickness direction. This results in two cases: three and two rings, with relaxation factors of 1.33 and 2, respectively. The calibrated stiffness parameters for the circumferential joints are reported in Table 2.

The load-displacement curves for the two load positions are shown in Figure 5. Based on the previous findings, the responses of the relaxed models with a relaxation factor of 2X (2 rings) differ significantly from the reference mesoscale models. The main difference is observed in the post-peak response, where hardening occurs instead of the softening behaviour predicted by the full mesoscale models, and peak loads are overestimated. In contrast, the relaxed models with 3 rings provide predictions that are closer to the responses of the full mesoscale models. In terms of secant stiffness, both relaxed models show reduced errors and improved results for the 3-ring models. The maximum error is 4% for the 3-ring models and 10% for the 2-ring models. When it comes to peak load, the differences in error percentages are much more significant. The error does not exceed 9% for the 3-ring model when the load is applied at quarter span, compared to a maximum error of 26% for the 2-ring model. At mid-span, the difference becomes even more significant, with an error of 22% for the 3-ring model compared to 127% for the 2-ring model. These results demonstrate how the relaxed models with 3 rings provide significantly improved responses.

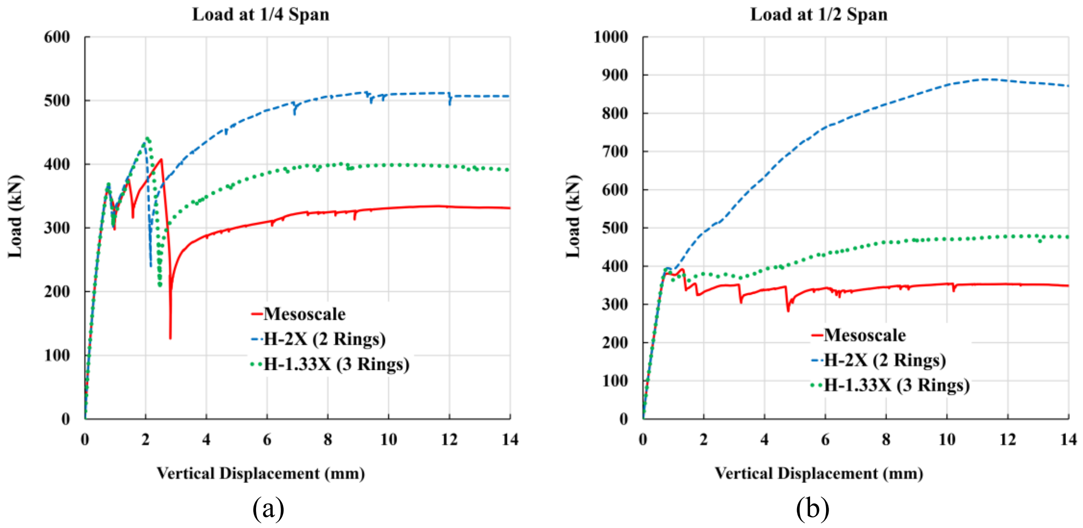

Figure 5: Load-displacement curves for different 2D relaxed mesoscale models along the thickness direction (H) with reference to the full mesoscale models under vertical load applied at (a) quarter; (b) mid-span.

Building on the results of the relaxed 2D strip models, the study has been extended to include full 3D models that consider all bridge components (arch, backfill, and spandrel walls). For this task, a 3 m span bridge with 3 m width is analysed. The arch barrel comprises two rings with a stretcher bond, having a total thickness of 215 mm. The backfill height above the crown is 300 mm as depicted in Figure 6. For spandrel walls, a thickness of 440 mm (composed of 4 half-bricks) is considered, with the walls constructed attached to the top of the arch barrel, following the English bond pattern. The load is applied using a patch load area of 750 × 750 mm^2 at quarter span, quarter width, causing significant damage and cracking in the spandrel walls.

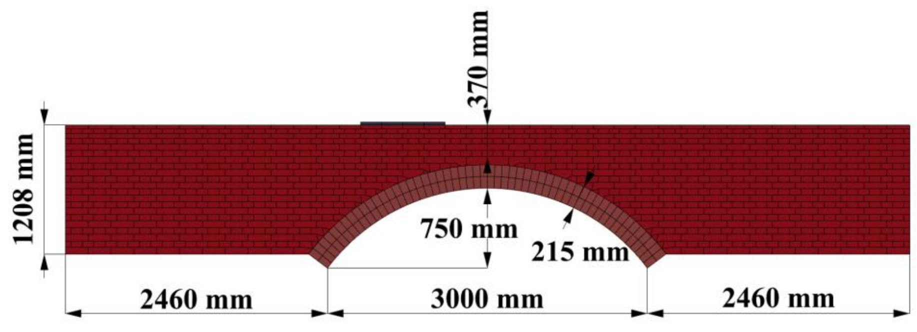

Figure 6: 3m span 2-ring bridge with 440 mm-thick attached spandrel walls.

For the arch barrel, a 2X relaxation is applied solely along the span and width directions. Conversely, given that the arch barrel comprises only two rings, relaxation along the thickness is inapplicable to a stretcher bond, which would otherwise be unable to represent potential ring separation. Compared to 2D strip models, including spandrel walls in the 3D model incurs significant computational effort, especially when a full mesoscale representation is adopted to account for their actual bond pattern. Consequently, relaxing the mesh for spandrel walls generally enhances computational efficiency, given their associated large number of degrees of freedom (DOFs). To study the influence of relaxation of the spandrel walls on the accuracy of the results, different forms of relaxation are considered, including relaxation along the span only (L), thickness only (W), and height only (H). This is followed by different relaxation combinations comprising relaxation along span and thickness (L&W), span and height (L&H), and thickness and height (W&H). Finally, a case with relaxation along span, thickness and height simultaneously (L&W&H) is considered. It is worth outlining that a relaxation factor of two (2X) is adopted in all these cases for the spandrel walls. Moreover, an additional relaxed model is investigated, where only one solid element is considered along the thickness direction of the spandrel walls. This renders the relaxation factor four times (4X) in thickness direction, while retaining the 2X relaxation factor along the span and height directions. The stiffness parameters adopted in both the full and relaxed mesoscale models are summarised in Table 3 for arch barrel and spandrel walls.

Component	Model	Span Direction		Width Direction		Height Direction	
		k_n [N/mm^3]	k_t [N/mm^3]	k_n [N/mm^3]	k_t [N/mm^3]	k_n [N/mm^3]	k_t [N/mm^3]
Arch Barrel	Mesoscale	295	118	295	118	-	-
	Relaxed 2X	137.71	55.13	141.83	56.73	-	-
Spandrel Walls	Mesoscale	295	118	295	118	295	118
	Relaxed 2X	159.8	63.64	147.5	59	149.58	59.76

Table 3: Stiffness parameters along the different directions of arch barrel and spandrel walls for the full and relaxed mesoscale models.

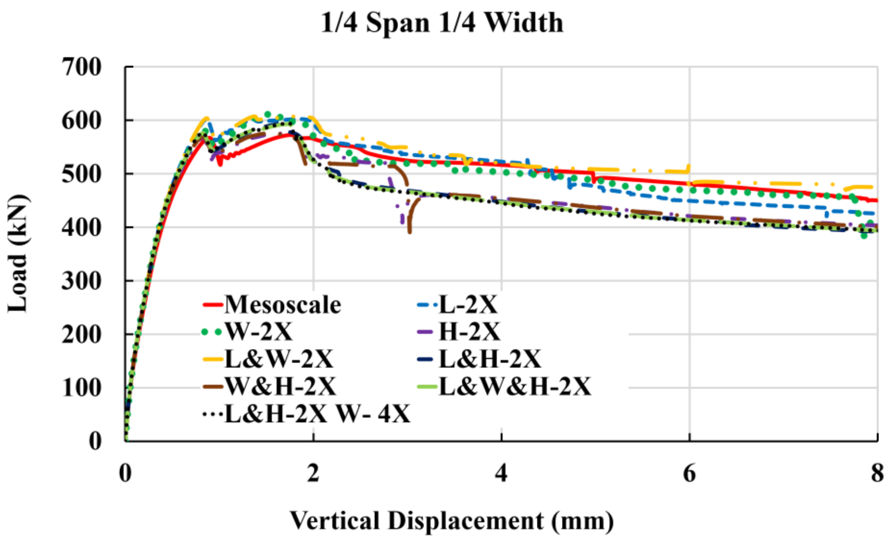

Figure 7. Load-displacement curves for different 3D relaxed models against the full mesoscale model under vertical load applied at quarter span quarter width.

Inspection of the load-displacement responses in Figure 7 shows excellent agreement between the reference full mesoscale model and the various relaxed models in terms of load capacity and secant stiffness. This is indicated by low error percentages, with maximum errors in peak load and secant stiffness of 7% and 12%, respectively. This excellent agreement also extends to the softening post-peak response for all relaxed cases, except those involving relaxation along the height (H) of the spandrel walls. For such cases, a slightly more degraded post-peak response is noted compared to the reference response.

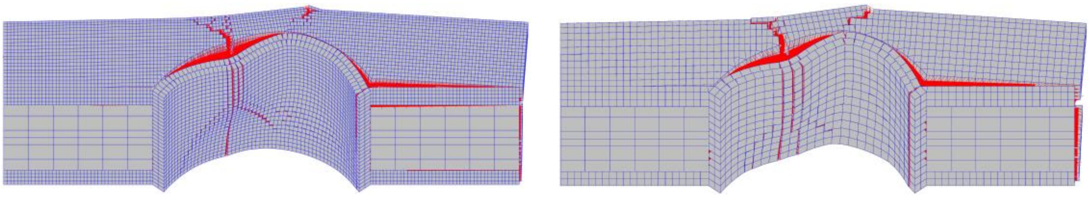

(a) (b)

Figure 8: Deformed shapes at failure for 3D bridge models: (a) full mesoscale; (b) relaxed L&W&H–2X under vertical load applied at quarter span quarter width.

Finally, the deformed shapes at failure for all the relaxed models considered show consistent failure modes relative to the reference full mesoscale model, as indicated in [39]. This is confirmed by the analogous crack pattern on the spandrel wall adjacent to the load, as outlined in Figure 8, which shows the deformed shapes for the full mesoscale and 2X-relaxed along (L&W&H) cases. The crack pattern features two stepped vertical cracks developing at the quarter and three-quarter spans due to downward and upward deformations of the arch barrel, resulting in two horizontal cracks within the spandrel walls near the arch springings. The first of those cracks is a major crack extending all the way along the base of the spandrel/wing wall in the unloaded half of the bridge. In contrast, the other crack is less significant, developing in the loaded part of the bridge covering a limited distance above the base of the spandrel wall. All these complex cracks are effectively captured by the relaxed model, showing high consistency with the full mesoscale model. Also, the cracking pattern in the relaxed arch barrel is close to the full mesoscale results.

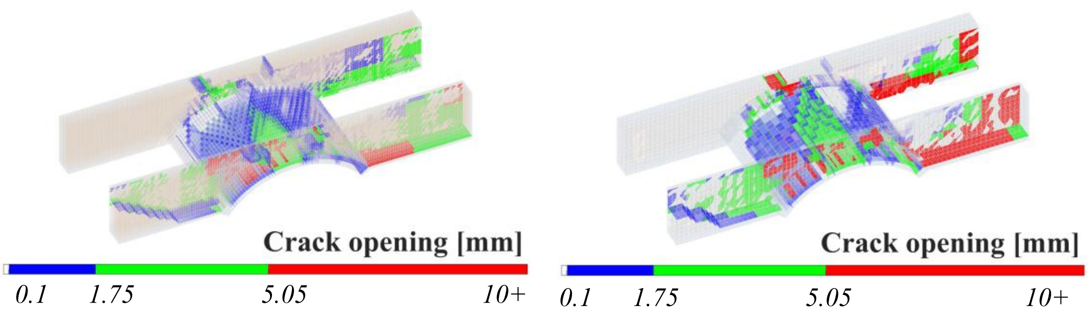

(a) (b)

Figure 9: Crack width distribution at collapse for 3D bridge models: (a) full mesoscale; (b) relaxed L&W&H–2X under vertical load applied at quarter span quarter width.

To further validate the accuracy of the relaxed models, the effect of model relaxation on predicting crack widths in 3D models is explored. The accuracy of crack width estimates is assessed using a colour map that highlights the locations and magnitudes of cracks. The same set of 3D bridge models investigated earlier is considered, with the crack width colour maps for the full and 2X-relaxed mesoscale models shown in Figure 9.

Predictions for the maximum crack width in relaxed models are reported in Table 4. It shows that the error in maximum crack width relative to the full mesoscale models does not exceed 11% across different forms of 2X relaxation along different directions of spandrel walls, which is satisfactorily accurate. It is also noted that relaxations along the span and thickness directions tend to slightly increase the error percentage compared to relaxation along the height direction. The last column in the table shows that considering only a single solid element along the thickness of the spandrel walls does not significantly reduce the accuracy of crack width predictions. This is confirmed by the low error percentage, which does not exceed 7%.

Model	Mesoscale	L–2X	W–2X	H–2X	L&W&H–2X	L&H–2X W–4X
Maximum crack width [mm]	19.3	21.3	21.1	18.8	20.6	20.6
Error w.r.t. full mesoscale	-	11%	10%	-3%	7%	7%

Table 4: Errors in maximum crack width for different 3D relaxed models with reference to the predictions of the baseline full mesoscale model.

After evaluating the accuracy of the relaxed mesoscale models in the previous sections, the computational efficiency is assessed herein by comparing the DOFs of the reduced models with those of the reference mesoscale models. In the 3D full mesoscale bridge model, Table 5 shows that the spandrel walls account for the majority of DOFs, as indicated by the number of nodes associated with the spandrel walls compared to those of the arch barrel and backfill. For the bridge with 440 mm-thick walls, the spandrel walls account for around 87% of the total number of nodes in the entire 3D model. Such a high percentage underscores the importance of accounting for relaxation within spandrel walls to improve the computational efficiency of 3D mesoscale models.

Table 5 summarises the reduction in DOFs for different forms of relaxation in the 440 mm-thick spandrel walls. In all these relaxed models, a 2X relaxation is applied to the arch barrel in both the span and width directions, while keeping the thickness direction unrelaxed. Focusing on spandrel walls, considering a relaxation factor of 2X along only the span, thickness, or height directions leads to a reduction of at least 51% in DOFs. Extending the 2X relaxation for spandrel walls to include two directions increases the reduction percentage to around 75% [39], which can be further increased to reach 84% when considering relaxation in the three directions simultaneously. Furthermore, maintaining a 2X relaxation in both the span and height directions while increasing the relaxation in the thickness direction to 4X results in a single solid element throughout the thickness of the spandrel wall. This leads to a further reduction in DOFs, reaching 90% in the relaxed model compared to the full mesoscale model.

Model	Number of Nodes			Number of DOFs	DOFs reduction
	Arch Barrel	Backfill	Single Spandrel Wall		
Full mesoscale	56160	4871	203640	1404933	-
L–2X	13520	4871	100360	657333	53%
W–2X	13520	4871	97020	637293	55%
H–2X	13520	4871	105800	689973	51%
L&W&H–2X	13520	4871	27380	219453	84%
L&H–2X W–4X	13520	4871	13690	137313	90%

Table 5: Assessment of computational efficiency for different 3D relaxed models against full mesoscale models in terms of number of DOFs.

4 Conclusions and Contributions

In this paper, reduced mesoscale models have been introduced as a simplified assessment method compared with detailed mesoscale models for masonry arch bridges. These relaxed models can offer both accuracy and computational efficiency while retaining most of the features of detailed models, including the prediction of crack evolution across different load levels. This investigation aims to contribute to the development of a multi-level modelling framework that connects simplified lower-level models to detailed mesoscale models. The motivation for this work stems from the high computational cost of detailed 3D models, which renders them unsuitable for practical use, especially when assessing large structures.

The calibration of the stiffness parameters of the interface elements representing the mortar joints in the relaxed models is crucial for achieving accurate predictions of the bridge stiffness. This, in turn, affects the ability of the relaxed models to predict crack widths at different loading levels up to collapse. However, a simple calibration procedure is proposed, focusing primarily on calibrating the stiffness parameters of the interface elements. This procedure provides a link between the relaxed and full mesoscale modelling strategies, in which the full mesoscale material parameters can be determined via material tests on the individual masonry constituents.

The accuracy of simplified mesoscale models has been assessed against the predictions of baseline full mesoscale models. The relaxed mesoscale models were found to be quite accurate even for highly relaxed meshes. They provided realistic predictions not only for the load-displacement responses and failure modes, but also for the distribution and magnitude of crack width in masonry components.

Relaxation along the arch barrel span and width directions yields accurate predictions of initial stiffness and peak load. Alternatively, relaxation along the thickness of the arch barrel should be considered only when the original structure has more than two rings, to allow for potential ring separation. In stretcher-bond arches with more than two rings, relaxation along the thickness direction leads to an overestimation of the peak load. To improve prediction accuracy, using at least three rings of solid elements along the arch thickness in the reduced mesoscale mesh is recommended.

Relaxation of the mesoscale mesh of the spandrel walls yields excellent results regardless of the direction, allowing relaxation in all three directions without affecting accuracy. Moreover, relaxing the spandrel walls by considering only a single solid element across their thickness has yielded precise predictions of the load-displacement responses and failure modes.

The relaxed mesoscale models have proven to be highly accurate and computationally cost-effective. These models have shown a significant reduction in the DOFs that can reach up to 90% depending on the adopted relaxation. This highlights the potential of adopting relaxed mesoscale models to achieve accurate predictions at a lower computational cost.

Acknowledgements

The authors acknowledge support from EPSRC grant EP/T001607/1 (Project title: Exploiting the resilience of masonry arch bridge infrastructure: a 3D multi-level modelling framework).

References

[1] Page J. Load tests to collapse on masonry arch bridges. Arch Bridges: Proceedings of the first international Conference on arch bridges. Bolton, UK Thomas Telford 1995. p. 289-98.

[2] Melbourne C, Gilbert M. The behaviour of multi-ring brickwork arch bridges. Structural Engineer. 1995;73:39-47.

[3] Melbourne C, Holm G, Bien J, Casas JR, Tommor A, Bengtsson PE et al. Masonry Arch Bridges: Sustainable Bridges Background document 4.7. 2007. p. 277.

[4] Wang J. The three-dimensional behaviour of masonry arches: University of Salford; 2004.

[5] Sarhosis V, Liu B, Gilbert M. The 3d response of a large-scale masonry arch bridge - part I: Performance under low and medium loading levels. Engineering Structures. 2024;316:118496.

[6] Liu B, Sarhosis V, Booth AD, Gilbert M. The 3D response of a large-scale masonry arch bridge – Part II: Performance at failure. Engineering Structures. 2024;313:118308.

[7] Zhang Y, Tubaldi E, Macorini L, Izzuddin BA. Mesoscale partitioned modelling of masonry bridges allowing for arch-backfill interaction. Construction and Building Materials. 2018;173:820-42.

[8] Tubaldi E, Macorini L, Izzuddin BA. Three-dimensional mesoscale modelling of multi-span masonry arch bridges subjected to scour. Engineering Structures. 2018;165:486-500.

[9] Grosman S, Bilbao AB, Macorini L, Izzuddin BA. Numerical modelling of three-dimensional masonry arch bridge structures. Proceedings of the Institution of Civil Engineers - Engineering and Computational Mechanics. 2021;174:96-113.

[10] El Ashri M, Grosman S, Macorini L, Izzuddin B. Numerical investigation of 3D response characteristics of masonry bridges by detailed mesoscale masonry models. 1 ed: CRC Press; 2023.
[11] Forgács T, Sarhosis V, Ádány S. Discrete element modelling of skew masonry arch bridges taking into account arch ring-backfill interaction. Proceedings of the International Masonry Society Conferences 10th International Masonry Conference. Milan, Italy: International Masonry Society; 2018. p. 337-46.
[12] Forgács T, Sarhosis V, Ádány S. 3D analysis of masonry arch bridges taking into account the spandrel walls. In: Billaux D, Hazzard J, Nelson M, Schöpfer M, editors.: Itasca International; 2020.
[13] Pulatsu B, Erdogmus E, Lourenço PB. Simulation of Masonry Arch Bridges Using 3D Discrete Element Modeling. Structural Analysis of Historical Constructions: Springer International Publishing; 2019. p. 871-80.
[14] Pulatsu B, Erdogmus E, Lourenço PB. Comparison of in-plane and out-of-plane failure modes of masonry arch bridges using discontinuum analysis. Engineering Structures. 2019;178:24-36.
[15] Liu B, Loverdos D, Sarhosis V. The 3D response of a large-scale masonry arch bridge: High-fidelity discrete element numerical analysis. Structures. 2026;89:112186.
[16] Gilbert M, Melbourne C. RIGID-BLOCK ANALYSIS OF MASONRY STRUCTURES. The Structural engineer. 1994;72.
[17] Heyman J. The masonry arch: Wiley; 1982.
[18] Papa T, Grillanda N, Milani G. Three-dimensional adaptive limit analysis of masonry arch bridges interacting with the backfill. Engineering structures. 2021;248:113189.
[19] Hua Y, Milani G. Full Modelling of Backfill in 3D Limit Analysis of Masonry Arch Bridges. Lecture Notes in Civil Engineering2025. p. 529-43.
[20] Scacco J, Grillanda N, Milani G, Lourenço PB. Novel non-linear static numerical model for curved masonry structures based on a combined adaptive limit analysis and discrete FE computations. International Journal of Solids and Structures. 2022;236-237:111265.
[21] Fanning PJ, Boothby TE. Three-dimensional modelling and full-scale testing of stone arch bridges. Computers & Structures. 2001;79:2645-62.
[22] Boothby TE, Roberts BJ. Transverse behaviour of masonry arch bridges. Structural Engineer. 2001;79:21-6.
[23] Hodgson JA. The behaviour of skewed masonry arch bridges: University of Salford; 1996.
[24] Milani G, Lourenco PB. 3D non-linear behavior of masonry arch bridges. Computers & Structures. 2012;110:133-50.
[25] Reccia E, Milani G, Cecchi A, Tralli A. Full 3D homogenization approach to investigate the behavior of masonry arch bridges: The Venice trans-lagoon railway bridge. Construction and Building Materials. 2014;66:567-86.
[26] Zizi M, Chisari C, De Matteis G. Influence of uncertain mechanical parameters on the load-bearing capacity of multi-span masonry arch bridges. CRC Press; 2023. p. 1538-45.
[27] Zizi M, Chisari C, De Matteis G. Effects of pre-existing damage on vertical load-bearing capacity of masonry arch bridges. Engineering Structures. 2024;300:117205.
[28] Pantò B, Chisari C, Macorini L, Izzuddin BA. A Macroscale Modelling Approach for Nonlinear Analysis of Masonry Arch Bridges. 12th International Conference on Structural Analysis of Historical Constructions. 2021.

[29] Pantò B, Chisari C, Macorini L, Izzuddin BA. A hybrid macro-modelling strategy with multi-objective calibration for accurate simulation of multi-ring masonry arches and bridges. Computers & Structures. 2022;265:106769.

[30] Pantò B, Macorini L, Izzuddin BA. A two-level macroscale continuum description with embedded discontinuities for nonlinear analysis of brick/block masonry. Computational Mechanics. 2022;69:865-90.

[31] Cannizzaro F, Pantò B, Caddemi S, Caliò I. A Discrete Macro-Element Method (DMEM) for the nonlinear structural assessment of masonry arches. Engineering Structures. 2018;168:243-56.

[32] Caddemi S, Caliò I, Cannizzaro F, D'Urso D, Occhipinti G, Pantò B et al. A 'parsimonious' 3D discrete macro-element method for masonry arch bridges. Proceedings of the International Masonry Society Conferences. 222279 ed2018. p. 541-51.

[33] Caddemi S, Caliò I, Cannizzaro F, D'Urso D, Pantò B, Rapicavoli D et al. 3D discrete macro-modelling approach for masonry arch bridges. IABSE Symposium, Guimaraes 2019: Towards a Resilient Built Environment Risk and Asset Management - Report2019. p. 1825-35.

[34] Bonatte M, Tubaldi E, Oliveira DV, Cannizzaro F, Rapicavoli D, Pantò B et al. A discrete macro-element method for structural assessment of masonry arch bridges. Engineering Structures. 2026;359:122757.

[35] Macorini L, Izzuddin BA. A non-linear interface element for 3D mesoscale analysis of brick-masonry structures. International Journal for Numerical Methods in Engineering. 2011;85:1584-608.

[36] Minga E, Macorini L, Izzuddin BA. Enhanced mesoscale partitioned modelling of heterogeneous masonry structures. International Journal for Numerical Methods in Engineering. 2017;113:1950-71.

[37] Izzuddin BA. Nonlinear dynamic analysis of framed structures: Imperial College London (University of London); 1991.

[38] Grosman S, Macorini L, Izzuddin BA. Parametric nonlinear modelling of 3D masonry arch bridges. Advances in Engineering Software. 2023;185:103514.

[39] El Ashri M. 3D Behaviour of Masonry Arch Bridges Using Multi-level Modelling: Imperial College London 2024.